Magnetoelastic and magnetostrictive properties of Co_2XAl Heusler compounds

Farzad Mahfouzi,[1,*] Gregory P. Carman,[2] and Nicholas Kioussis[1,†]
[1]*Department of Physics and Astronomy, California State University, Northridge, California 91330, USA*
[2]*Department of Mechanical and Aerospace Engineering, University of California, Los Angeles, California 90095, USA*

(Received 15 June 2020; revised 31 July 2020; accepted 19 August 2020; published 1 September 2020)

We present a comprehensive first-principles electronic structure study of the magnetoelastic and magnetostrictive properties in Co-based Co_2XAl (X = V, Ti, Cr, Mn, Fe) full Heusler compounds. In addition to the commonly used total energy approach, we employ the torque method to calculate the magnetoelastic tensor elements. We show that the torque-based methods are, in general, computationally more efficient and allow us to unveil the atomic and orbital contributions to the magnetoelastic constants in an exact manner, as opposed to the conventional approaches based on second-order perturbation with respect to the spin-orbit coupling. The magnetostriction constants are in good agreement with available experimental data. The results reveal that the main contribution to the magnetostriction constants, λ_{100} and λ_{111}, arises primarily from the strain-induced modulation of the $\langle d_{x^2-y^2}|\hat{L}_z|d_{xy}\rangle$ and $\langle d_{z^2}|\hat{L}_x|d_{yz}\rangle$ spin-orbit coupling matrix elements, respectively, of the Co atoms.

DOI: 10.1103/PhysRevB.102.094401

I. INTRODUCTION

The development of efficient and scalable means to manipulate the magnetic state has been one of the main foci of scientific research in the field of condensed-matter physics and material science in the past century. The use of magnetoelastic materials employed in multiferroic heterostructures offers a promising avenue for efficient, scalable, and nonvolatile magnetic-based memory devices [1]. Magnetoelasticity is a phenomenon in which a deformation of the crystal shape results in a change in magnetic orientation and vice versa. In addition to applications in multiferroic-based magnetic memory devices, compounds with a large magnetoelastic constant are also of great interest in the development of efficient magnetomechanical actuators [2], magnetic field sensors, strain-mediated miniaturized multiferroic-based antennas, and other energy converter devices [3–5]. Therefore, development of a concise and efficient framework to calculate the magnetoelastic constants and understand their microscopic origin is of paramount importance in the search for magnetoelastic materials [6–8].

Even though rare-earth 3d metal compounds, such as Terfenol-D, exhibit the highest magnetostriction values (1500–2000 ppm) at room temperature, their use in industrial applications is hindered by the need for high-saturation magnetic field (due to their large magnetocrystalline anisotropy), brittleness, and high material costs [9]. Subsequently, highly magnetostrictive rare-earth-free Fe-based alloys were developed, such as $Fe_{1-x}Ga_x$ (galfenol) [10,11] and $Fe_{1-x}Al_x$ (alfenol) [12], which display large strain at moderate field and excellent ductility. In addition, spinel ferrites ($CoFe_2O_4$, $NiFe_2O_4$) with large magnetostriction [7] and high magnetic ordering temperatures were recently used in magnetostrictive-piezoelectric composites to enhance the interfacial magnetoelectric coupling [13].

Another remarkable class of materials is the Heusler ternary intermetallic compounds that crystallize in the $L2_1$ structure and have stoichiometric composition of X_2YZ (space group $Fm\bar{3}m$), where X and Y are transition metal elements and Z is an element from the p block [14,15]. They show a wide range of remarkable properties such as half-metallicity [14], high Curie temperatures [16], giant tunnel magnetoresistance [17,18], magnetic shape memory [19], superconductivity [20], topological Weyl fermions [14,21,22], and the anomalous Nernst effect [23]. More specifically, the cobalt-based Heusler compounds such as Co_2XAl (X = Ti, V, Cr, Mn, Fe) offer an interesting playground for spintronics applications since they have high Curie temperatures and some of them are predicted to be half-metallic ferromagnets [14,15]. Nevertheless, their magnetoelastic and magnetostrictive properties remain unexplored both experimentally and theoretically.

Here, we provide a general framework in which we employ different approaches to calculate the magnetoelastic and magnetostriction tensor elements of Co_2XAl (X = V, Ti, Cr, Mn, Fe) full Heusler compounds from first-principles electronic structure calculations. The first one is the well-known approach based on total energy calculations, and the other two are based on the torque and spin-orbital torque methods. We show that the torque-based methods are computationally more efficient and allow for the atomic and orbital decomposition of the magnetoelastic constants, which can, in turn, elucidate the underlying atomic mechanisms.

II. THEORETICAL FORMALISM

A. Magnetocrystalline anisotropy

The origin of the magnetocrystalline anisotropy (MCA) energy is the spin-orbit interaction and can be determined,

*Farzad.Mahfouzi@gmail.com
†nick.kioussis@csun.edu

within density-functional theory, from the second-variation method employing the scalar-relativistic eigenfunctions of the valence states [24,25]. In first-principles electronic structure calculations two approaches are often used to calculate the MCA, namely, the total energy and torque methods.

Total energy approach. The total energy $E_{\rm tot}(\vec{m})$ is determined for several magnetic orientations described by the unit vector $\vec{m}$, which in turn is fitted to lowest order in the magnetic degrees of freedom, given by

$$E_{\rm tot}(\vec{m}) = E^0_{\rm tot} + \sum_{ij} K^{ij} m_i m_j. \tag{1}$$

Here, K^{ij} are the MCA tensor matrix elements, and m_i are the components of the magnetization orientation unit vector $\vec{m}$.

As an alternative approach, instead of the total energy, one can employ the so-called force theorem [26], in which the dependence of the electronic energy on the magnetization directions can be approximately expressed in terms of the band energies $E_{\rm band}(\vec{m})$ (the sum of occupied one-electron eigenvalues), namely,

$$E_{\rm band}(\vec{m}) = \frac{1}{N_k}\sum_{n\vec{k}} \epsilon^{\vec{m}}_{n\vec{k}} f\big[\epsilon^{\vec{m}}_{n\vec{k}} - \mu(\vec{m})\big]. \tag{2}$$

Here, $f(x)$ is the Fermi-Dirac distribution function, N_k is the number of k points, and $\mu(\vec{m})$ is the electronic chemical potential which depends on the magnetization direction.

Torque approach. Wang *et al.* proposed [27] a torque method for the theoretical determination of the MCA energy for systems with uniaxial symmetry that, instead of directly calculating the total energy difference, involves the expectation value of the angular derivative of the spin-orbit coupling (SOC) Hamiltonian at an angle $\theta = 45^\circ$,

$$T(\theta) = \sum_{n\mathbf{k}}^{\rm occ} \big\langle \Psi^{\rm SOC}_{n\mathbf{k}} \big| \frac{\partial H^{\rm SOC}}{\partial \theta} \big| \Psi^{\rm SOC}_{n\mathbf{k}} \big\rangle_{\theta=45^\circ}. \tag{3}$$

Here, $\Psi^{\rm SOC}_{n\mathbf{k}}$ is the nth relativistic eigenvector at the $\mathbf{k}$ point, and θ is the angle between the magnetization direction and the surface normal.

The one-electron Kohn-Sham Hamiltonian can be expressed as [28,29]

$$\hat{H} = \hat{H}_K(\vec{k})\hat{1}_{2\times 2} + \hat{\Delta}(\vec{k})\vec{m}\cdot\vec{\sigma} + \hat{H}_{\rm soc}(\vec{k}), \tag{4}$$

where the first, second, and third terms represent the kinetic, exchange, and SOC contributions, respectively. In a nonorthonormal atomic-orbital basis set, the eigenenergies and eigenstates are calculated from the generalized eigenvalue problem, $\hat{H}|n\vec{k}\rangle = \epsilon_{n\vec{k}}\hat{\mathcal{O}}|n\vec{k}\rangle = \epsilon_{n\vec{k}}\mathcal{O}_{n\vec{k}}|n\vec{k}\rangle$, where $\hat{\mathcal{O}}(\vec{k})$ is the overlap matrix. In this case, the torque is given by [28]

$$\vec{\tau}_{\rm MCA} = -\vec{m}\times\langle\hat{\Delta}\vec{\sigma}\rangle, \tag{5}$$

where the equilibrium expectation value is calculated from

$$\langle\cdots\rangle = \frac{1}{N_k}\sum_{n\vec{k}}\langle n\vec{k}|\cdots|n\vec{k}\rangle\frac{f(\epsilon_{n\vec{k}}-\mu_0)}{\mathcal{O}_{n\vec{k}}}. \tag{6}$$

Unlike the total energy method, the torque approach involves a vector for the fitting to the magnetization orientation, and also it does not require the calculation of a reference energy, making it computationally more efficient. Furthermore, the torque method can be used to calculate the local (site-resolved) contribution to the MCA energy since the exchange splitting $\hat{\Delta}$ is often a well-defined local quantity.

In this paper, instead of the aforementioned torque method we employ a different approach we recently developed [30] based on the canonical forces, $F_\theta = \vec{n}\cdot\vec{\tau} = -\langle\frac{\partial\hat{H}}{\partial\theta}\rangle$ and $F_\phi = \vec{e}_z\cdot\vec{\tau} = -\langle\frac{\partial\hat{H}}{\partial\phi}\rangle$, where θ (ϕ) is the polar (azimuthal) angle, $\vec{n} = \sin\phi\vec{e}_x - \cos\phi\vec{e}_y$, and $\vec{e}_z$ is the unit vector along z. Applying the unitary operator $\hat{U} = e^{i\theta\vec{n}\cdot\vec{\sigma}/2}$ on the Hamiltonian to reorient the exchange splitting term along the z axis, we find

$$F_q = 2{\rm Re}\Big\langle \hat{U}\frac{\partial\hat{U}^\dagger}{\partial q}\hat{H}_{\rm soc}\Big\rangle, \quad q = \theta, \phi. \tag{7}$$

Using Eq. (7) for $q = \theta$, one can obtain an explicit expression for the MCA-induced torque,

$$\vec{\tau}_{\rm MCA} = \langle\hat{\xi}\vec{\hat{L}}\times\vec{\sigma}\rangle, \tag{8}$$

which we refer to as the "spin-orbital" torque approach [29,30] as opposed to the original torque method given by Eq. (5). It should be pointed out that Eq. (8) is exact and no approximation was involved in its derivation.

Equation (8) can be interpreted as the torque induced by the anisotropic orbital moment accumulation $\vec{\hat{L}}$ on the spin $\vec{\sigma}$ of the valence electrons. Since the SOC strength $\hat{\xi}$ is diagonal in the atomic-orbital basis set and a well-defined local quantity, we can use Eq. (8) to decompose the torque on each atom. This decomposition allows us, in turn, to elucidate the atomic origin of the MCA as opposed to the local MCA-induced field on each atomic spin given by Eq. (5). Therefore, the advantage of using Eqs. (7) and (8) is that they allow us to unveil the underlying origin of the MCA. Employing Eq. (8), the atom and orbital contributions to the total torque can be written as

$$\langle\alpha|\vec{\tau}^I_{\rm MCA}|\beta\rangle = \sum_{ss'}\rho^{I,\alpha\beta}_{ss'}\langle I\alpha s|\hat{\xi}\vec{\hat{L}}\times\vec{\sigma}|I\beta s'\rangle, \tag{9}$$

where I is the atomic index, α, β (s, s') are the orbital (spin) indices, and

$$\rho^{I,\alpha\beta}_{ss'} = \frac{1}{N_k}\sum_{n\vec{k}}\langle I\beta s'|n\vec{k}\rangle\frac{f(\epsilon_{n\vec{k}}-\mu_0)}{\mathcal{O}_{n\vec{k}}}\langle n\vec{k}|I\alpha s\rangle \tag{10}$$

is the density matrix.

B. Magnetoelastic effect

Magnetoelastic coupling is the interaction between the magnetization and the strain in a magnetic material. In the presence of strain ε_{ij}, the modified primitive lattice vectors $\vec{a}'_i$ are given by $(\vec{a}'_i - \vec{a}_i)\cdot\vec{e}_j = \sum_k \vec{a}_i\cdot\vec{e}_k\varepsilon_{kj}$, where $\vec{e}_j$ represent unit vectors in Cartesian coordinates. To lowest order in the lattice deformation (i.e., small strain) and magnetization orientation, the total energy per equilibrium volume is given by

$$E(\vec{m}) = E_0 + \frac{1}{2}\sum_{i\leqslant j,k\leqslant l} C^{ij}_{kl}\varepsilon_{ij}\varepsilon_{kl} + \sum_{ij} K^{ij}(\{\varepsilon_{kl}\})m_i m_j, \tag{11}$$

where C_{kl}^{ij} are the elastic stiffness constants, often represented by a 6×6 matrix. To linear order in strain, the MCA tensor matrix elements have the form $K^{ij}(\{\varepsilon_{kl}\}) = K_0^{ij} + \sum_{k\leqslant l} B_{kl}^{ij}\varepsilon_{kl}$, where B_{kl}^{ij} denote the magnetoelastic tensor elements.

The magnetostriction effect, first identified in 1842 by Joule [31], is a property of ferromagnetic materials that causes them to change their shape when subjected to a magnetic field. In the absence of an external stress, the strain induced on the crystal structure due to the reorientation of the magnetization can be calculated by setting $\partial E(\vec{m})/\partial\varepsilon_{kl} = 0$,

$$\varepsilon_{kl} = -\sum_{kl} h_{kl}^{ij} m_i m_j, \tag{12}$$

where $h_{kl}^{ij} = \sum_{k'\leqslant l'} S_{kl}^{k'l'} B_{k'l'}^{ij}$ are the magnetostriction tensor elements and S_{kl}^{ij} are the elastic compliance constants. Under the applied strain ε_{ij}, the relative change in the length of the material $\delta l/l$ along a direction given by the unit vector $\vec{u}$ can be calculated [32,33] by $\delta l/l = \sum_{ij} \varepsilon_{ij} u_i u_j$. Using Eq. (12) for the strain, the relative change in the length due to the reorientation of the magnetization can be calculated by

$$\frac{\delta l}{l} = -\sum_{ijkl} h_{kl}^{ij} u_i u_j m_k m_l. \tag{13}$$

Given that the components of the unit vectors $\vec{u}$ and $\vec{m}$ describing the directions of the relative change in the length and magnetization, respectively, are not independent, the basis set in Eq. (13) consisting of $u_i u_j$ and $m_i m_j$ is overcomplete. One approach to resolve this issue is to switch to the spherical Harmonics basis set [34], which is more advantageous, especially when dealing with ensemble averaging. In the following we use this approach to obtain a general expression for the polycrystalline magnetostriction constant. Using the second-order spherical Harmonics, we can rewrite Eq. (13) in the form

$$\frac{\delta l}{l} = \sqrt{\frac{4\pi}{5}} \sum_p \lambda_p^{(0)} Y_{2,p}(\vec{m}) + \frac{4\pi}{5} \sum_{pq} \lambda_{pq}^{(2)} Y_{2,p}(\vec{m}) Y_{2,q}(\vec{u}), \tag{14}$$

where the isotropic (volumetric) magnetostriction constant $\lambda_p^{(0)}$ $(p = 1, \ldots, 5)$ and anisotropic magnetostriction constants $\lambda_{pq}^{(2)}$ can be expressed (see the Appendix) in terms of h_{kl}^{ij} and $Y_{2,p}$ are the real spherical harmonics, given by

$$Y_{2,p}(\vec{r}) = \sqrt{\frac{15}{4\pi}} \left(\frac{x^2 - y^2}{2}, \frac{3z^2 - 1}{2\sqrt{3}}, yz, xz, xy \right). \tag{15}$$

For a polycrystalline structure the field-induced relative change in the length has the form $\delta l/l = \lambda_s P_2(\vec{m} \cdot \vec{u})$, where $P_2(x)$ denotes the Legendre polynomials of order 2. Therefore, the average magnetostriction constant λ_s can be calculated by

$$\lambda_s = \frac{5}{(4\pi)^2} \iint d\Omega_{\vec{m}} d\Omega_{\vec{u}} \frac{\delta l}{l} P_2(\vec{m} \cdot \vec{u}) = \frac{1}{5} \sum_p \lambda_{pp}^{(2)}. \tag{16}$$

For a cubic crystal structure the magnetostriction constant matrix $\lambda_{pq}^{(2)}$ is diagonal, and the magnetic-field-induced shape deformation is given by

$$\frac{\delta l}{l} = \frac{4\pi}{5} \left[\lambda_{[100]} \sum_{p=1,2} Y_{2,p}(\vec{u}) Y_{2,p}(\vec{m}) + \lambda_{[111]} \sum_{p=3,4,5} Y_{2,p}(\vec{u}) Y_{2,p}(\vec{m}) \right]. \tag{17}$$

In this case, for the polycrystalline magnetostriction constant we obtain $\lambda_s = (2\lambda_{[100]} + 3\lambda_{[111]})/5$ [32].

III. COMPUTATIONAL APPROACHES

We have employed two *ab initio* electronic structure codes to determine the magnetoelastic tensor elements. The first is the plane wave Vienna *ab initio* Simulation Package (VASP) [35,36], where we have employed the total energy approach. The second is the linear combination of atomic orbitals (LCAO) OPENMX package [37–39], where one can employ any of the four approaches, namely, the total energy, the band energy [Eq. (2)], the torque [Eq. (5)], or the spin-orbital torque [Eq. (8)] approach. Throughout the remainder of the paper all OPENMX results employ the more computationally efficient spin-orbital torque approach.

(1) Structural relaxations were carried out using VASP [35,36] within the generalized gradient approximation as parameterized by Perdew, Burke, and Ernzerhof [40] (PBE) when the largest atomic force is smaller than 0.01 eV Å^{-1}. The pseudopotential and wave functions are treated within the projector augmented-wave method [41,42]. The plane wave cutoff energy was set to 500 eV, and an 18^3 k-point mesh was used in the Brillouin zone (BZ) sampling. Total energy calculations were carried out for nine different magnetization orientations, $\vec{m} = [1,0,0]$, $[0,1,0]$, $[0,0,1]$, $[1,1,0]$, $[1,\bar{1},0]$, $[1,0,1]$, $[1,0,\bar{1}]$, $[0,1,1]$, and $[0,1,\bar{1}]$. The MCA tensor elements in Eq. (11) were then calculated by

$$K^{zz} = 0, \tag{18a}$$

$$K^{xx} = E^{[1,0,0]} - E^{[0,0,1]}, \tag{18b}$$

$$K^{yy} = E^{[0,1,0]} - E^{[0,0,1]}, \tag{18c}$$

$$K^{xy} = \frac{E^{[1,1,0]} - E^{[1,\bar{1},0]}}{2}, \tag{18d}$$

$$K^{yz} = \frac{E^{[0,1,1]} - E^{[0,1,-1]}}{2}, \tag{18e}$$

$$K^{xz} = \frac{E^{[1,0,1]} - E^{[1,0,-1]}}{2}. \tag{18f}$$

(2) Using the lattice parameters determined from VASP calculations, the tight-binding Hamiltonian $\hat{H}_{\vec{k}}$ and overlap $\hat{O}_{\vec{k}}$ matrices were calculated in the LCAO OPENMX package [37–39]. We adopted the Troullier-Martins-type norm-conserving pseudopotentials [43] with partial core correction. We used 24^3 k points in the first BZ and an energy cutoff of 350 Ry for numerical integrations in the real-space grid. For the exchange correlation functional the Local Spin Density Approximation (LSDA) [44] parameterized by Perdew and Zunger [45] was used. The MCA tensor elements K_{ij} are determined via the spin-orbital torque [Eq. (8)] method

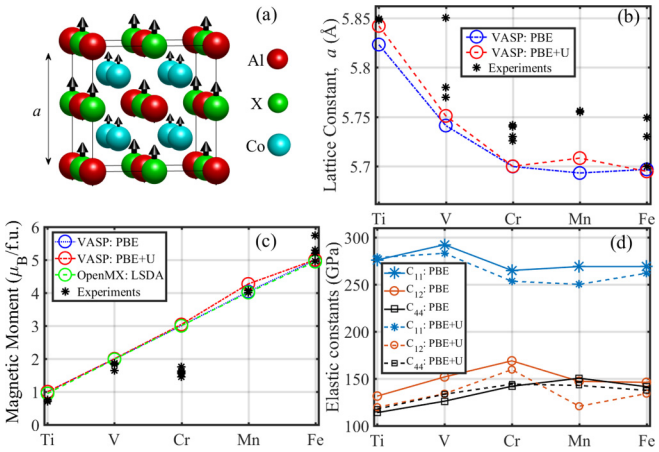

FIG. 1. (a) $L2_1$ crystal structure of full Heusler compounds. (b) Lattice constants of Co_2XAl compounds using the PBE exchange correlation functional with (red circles) and without (blue circles) Hubbard U included [46]. The stars show experimental data reported in [47–62]. (c) Total magnetic moment per formula unit versus X elements using VASP (blue and red symbols) and OPENMX (green symbols). The experimental results shown as black stars for X=Ti, V, Cr, Mn, and Fe have been reported in [47,48], [49–51], [52–57], [58,59], and [52,60–62], respectively. (d) Elastic constants C_{11}, C_{12}, and C_{44} calculated using the PBE (dashed lines) and PBE+U (solid lines) exchange-correlation functionals in VASP.

for three magnetization directions, $\vec{m}$ =[1,0,0], [1,0,1], and [0,1,1], from the expressions

$$\vec{\tau}^{[100]}_{\rm MCA} = [0, 2K^{xz}, -2K^{xy}], \tag{19a}$$

$$\vec{\tau}^{[101]}_{\rm MCA} = [K^{xy} + K^{yz}, K^{zz} - K^{xx}, -K^{xy} - K^{yz}], \tag{19b}$$

$$\vec{\tau}^{[011]}_{\rm MCA} = [K^{yy} - K^{zz}, -K^{xy} - K^{xz}, K^{xy} + K^{xz}]. \tag{19c}$$

The magnetoelastic constant tensor elements B^{kl}_{ij} are determined from MCA calculations under 12 strain ε_{ij} values of $\varepsilon_{xx} = \pm\delta_\varepsilon$, $\varepsilon_{yy} = \pm\delta_\varepsilon$, $\varepsilon_{zz} = \pm\delta_\varepsilon$, $\varepsilon_{xy} = \pm\delta_\varepsilon$, $\varepsilon_{yz} = \pm\delta_\varepsilon$, $\varepsilon_{xz} = \pm\delta_\varepsilon$, where $\delta_\varepsilon = 0.01$. The magnetoelastic constant tensor elements are then simply given by

$$B^{ij}_{kl} = \frac{K^{ij}(\varepsilon_{kl} = \delta_\varepsilon) - K^{ij}(\varepsilon_{kl} = -\delta_\varepsilon)}{2\delta_\varepsilon}. \tag{20}$$

It should be noted that the symmetry of the crystal structure can significantly reduce the number of independent configurations (induced strain and magnetization directions) required to obtain the magnetoelastic tensor elements. In particular, in cubic systems, only two nonzero independent magnetoelastic constants exist that are referred to as $B_1 = B^{xx}_{xx} = B^{yy}_{yy} = -B^{xx}_{zz} = -B^{yy}_{zz}$ and $B_2 = B^{xy}_{xy} = B^{yz}_{yz} = B^{zx}_{zx}$, constants corresponding to the normal and shear-induced MCAs, respectively.

IV. RESULTS AND DISCUSSION

The Heusler compounds Co_2XAl crystallize in the cubic $L2_1$ structure (space group $Fm\bar{3}m$) which is shown in the inset of Fig. 1(a). The Co atoms occupy Wyckoff position 8c (1/4, 1/4, 1/4); the X and Al atoms are located at 4a (0, 0, 0) and 4b (1/2, 1/2, 1/2), respectively. As depicted in Fig. 1(a), this structure consists of four interpenetrating fcc sublattices, two of which are equally occupied by X [14,15].

The calculated lattice constants shown in Fig. 1(b) demonstrate a monotonic decrease with increasing atomic number of the X element, consistent with their corresponding atomic radius. We have also carried out PBE+U calculations where we used the values of U for the d orbitals of Co and the X elements from Ref. [46]. The effect of U on the lattice constants [blue dashed curve in Fig. 1(b)] shows a slight increase of the lattice constant when compared to the case without U. The results are in good agreement with the experimentally reported data [47–62], denoted by black stars in Fig. 1(b). Heusler compounds are known for their well-behaved magnetic properties in terms of their total number of valence electrons. The total magnetic moment per formula unit is shown in Fig. 1(c) versus the X element (sorted with respect to its atomic number). In agreement with the Slater-Pauling curve [63], the magnetic moment per formula unit is an integer number that depends linearly on the number of valence electrons per formula unit N_v, given by $M_s = N_v - 24$ ($M_s = 34 - N_v$) for $X \leqslant$ Fe ($X \geqslant$ Fe). Surprisingly, the results are relatively insensitive to the exchange correlation functional (PBE, PBE+U, or LSDA), and except for Co_2CrAl, the *ab initio* results are in relatively good agreement with the experimentally reported findings in Refs. [47–62]. The slight increase of the magnetic moment in Co_2MnAl due to the inclusion of U is in agreement with previous density functional theory (DFT) calculations [46]. The origin of the discrepancy in the case of Co_2CrAl is attributed to $B2$-like disorder and an antiferromagnetic coupling of Cr with its neighbors, leading to ferrimagnetic behavior [64].

For cubic crystal structures the elastic energy is given by

$$E_{el} = \tfrac{1}{2}C_{11}\left(\varepsilon^2_{xx} + \varepsilon^2_{yy} + \varepsilon^2_{zz}\right) + \tfrac{1}{2}C_{44}\left(\varepsilon^2_{xy} + \varepsilon^2_{yz} + \varepsilon^2_{xz}\right) + C_{12}(\varepsilon_{xx}\varepsilon_{yy} + \varepsilon_{yy}\varepsilon_{zz} + \varepsilon_{xx}\varepsilon_{zz}), \tag{21}$$

where the subscripts in C_{ij} correspond to the Voigt notation ([1, 2, 3, 4, 5, 6] $\equiv$ [xx, yy, zz, yz, xz, xy]). In Fig. 1(d) we present the calculated (using VASP) elastic constants C_{11}, C_{12}, and C_{44} versus X elements. The results are in good agreement with previous first-principles electronic structure calculations [65]. The solid (dashed) lines in Fig. 1(d) correspond to the DFT calculations without (with) the Hubbard U term. The inclusion of U results in an overall decrease of the C_{11} and C_{12} elastic constants and a small change in C_{44}. Elastic stability of a compound requires that all eigenvalues of the 6×6 elastic matrix be positive. For a cubic crystal structure the eigenvalues are C_{44}, $C_{11} + 2C_{12}$, and $C_{11} - C_{12}$, corresponding to shear, bulk, and tetragonal shear moduli, respectively. The results for the elastic constants presented in Fig. 1(b) demonstrate that all compounds are stable under any elastic deformation.

The magnetoelastic energy for a cubic crystal structure is given by [32]

$$E_{me} = B_1\left(\varepsilon_{xx}m^2_x + \varepsilon_{yy}m^2_y + \varepsilon_{zz}m^2_z\right) + B_2(\varepsilon_{xy}m_xm_y + \varepsilon_{yz}m_ym_z + \varepsilon_{xz}m_xm_z). \tag{22}$$

Figure 2 shows the magnetocrystalline anisotropy tensor matrix elements K^{xx} and K^{xy} as a function of strains ε_{xx} and

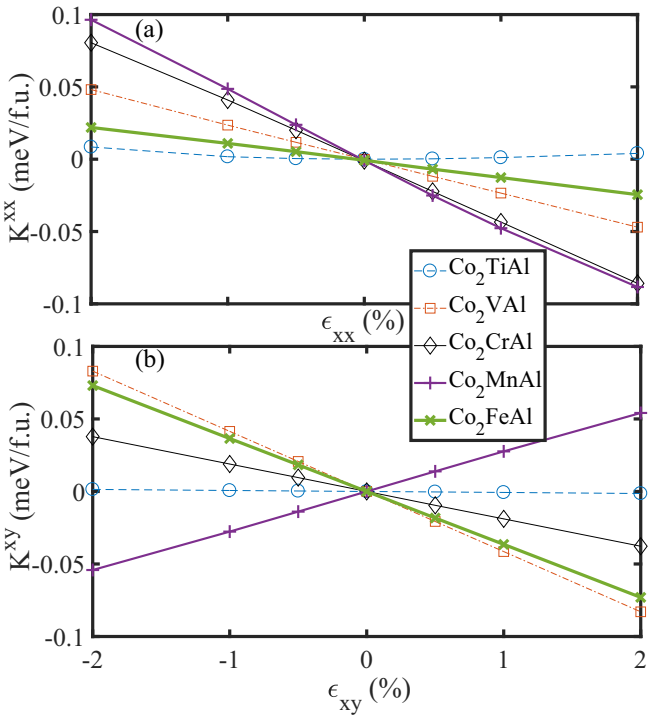

FIG. 2. Strain dependence of magnetocrystalline anisotropy coefficients K^{xx} and K^{xy} calculated from the "spin-orbital" torque approach under ε_{xx} and ε_{xy} strains, respectively, for the Co_2XAl (X = Ti, V, Cr, Mn, Fe) family.

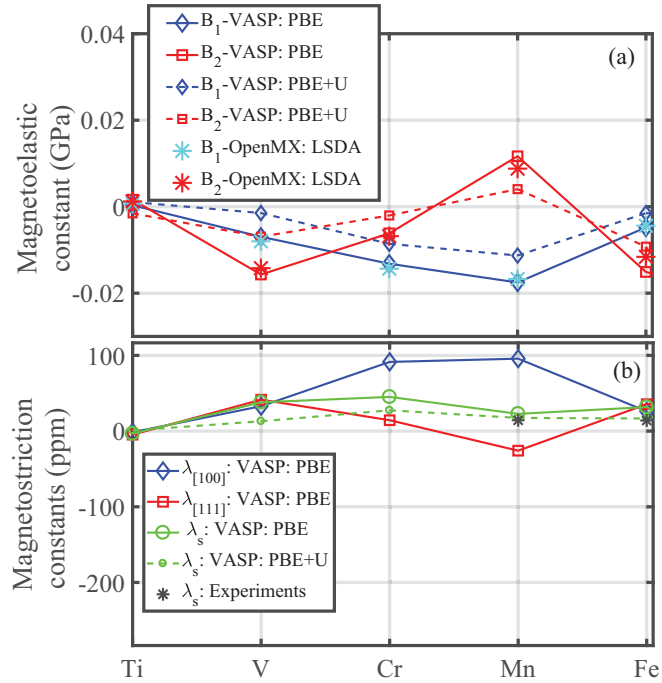

FIG. 3. (a) Magnetoelastic constants B_1 (blue symbols) and B_2 (red symbols) versus X elements in Co_2XAl Heusler compounds, calculated using VASP with the PBE exchange correlation (solid lines) and PBE+U (dashed lines). We have also included the results of the calculation using OPENMX with the LSDA exchange correlation functional (stars). (b) Magnetostriction constants $\lambda_{[100]}$ and $\lambda_{[111]}$ (using VASP with PBE) and the average magnetostriction for polycrystalline systems λ_s versus X elements. The dashed line corresponds to the polycrystalline magnetostriction calculated using VASP with PBE+U. For comparison we also show the experimental values (black stars) for Co_2MnAl [66] and Co_2FeAl [67] at room temperature.

ε_{xy}, respectively, for the Co_2XAl Heusler compounds using the spin-orbital torque approach with the OPENMX DFT package. As expected, the strain dependence is linear within the range of -2% to $+2\%$, suggesting that two strain values, as implemented in Eq. (20), are sufficient to calculate the magnetoelastic coefficients accurately. Note that $dK^{xx}/d\varepsilon_{xx} < 0$ for all compounds. On the other hand, the variation of $dK^{xy}/d\varepsilon_{xy}$ across the series is nonmonotonic and is discussed in detail below.

Figure 3(a) displays the magnetoelastic constants B_1 and B_2 versus the X element, shown as blue and red symbols, respectively. The solid (dashed) lines in Fig. 3(a) are the results of VASP calculations using PBE without (with) the U term, while the stars are calculated using OPENMX with the LSDA exchange correlation functional. We find overall good agreement between the results of the two different *ab initio* packages. The effect of U is to reduce both magnetoelastic constants by a factor of 2.

Figure 3(a) shows that the magnetoelastic constant B_1 is negative for all members of the Co_2XAl family independent of the exchange correlation functionals, and ignoring the effect of Hubbard U, it ranges from around -20 to 0 MPa, comparable to the corresponding range for the spinel ferrites $CoFe_2O_4$ and $NiFe_2O_4$ [7]. The magnetoelastic coupling constants B_2 range from about -15 to $+10$ MPa, which are higher by an order of magnitude than the corresponding values for the spinel ferrites. In Fig. 3(b) we show the magnetostriction constants $\lambda_{[100]}$ and $\lambda_{[111]}$ and the average magnetostriction constant λ_s, suitable for polycrystalline systems, versus the X element. The polycrystalline magnetostriction constant using PBE+U (dashed green curve) is approximately 50% lower than the corresponding values without U (solid green curve). Since the difference between the magnetoelastic constants obtained from VASP and OPENMX is small, we show in Fig. 3(b) only the magnetostriction constants calculated from VASP. For comparison we also display the available experimental values of λ_s for Co_2MnAl [66] and Co_2FeAl [67]. Overall, the DFT+U results are in better agreement with the experimentally reported room-temperature values. It should be noted that since thermal spin and phonon fluctuations are not taken into account in the DFT calculations, one should not expect very good agreement between the theoretical results and the reported experimental values at room temperature.

To understand the underlying origin of the magnetoelastic properties across the series we have used Eq. (9) employed in the OPENMX DFT package to resolve the total torque into its atomic and orbital contributions. In Figs. 4(a) and 4(b) [Figs. 4(c) and 4(d)] we show the orbital and atomic contributions to the magnetoelastic constant K^{xx} (K^{xy}) versus X elements. The MCA constants originate primarily from the Co and X elements, shown in the left and right panels, respectively. On the left-hand ordinate in Fig. 4 we display

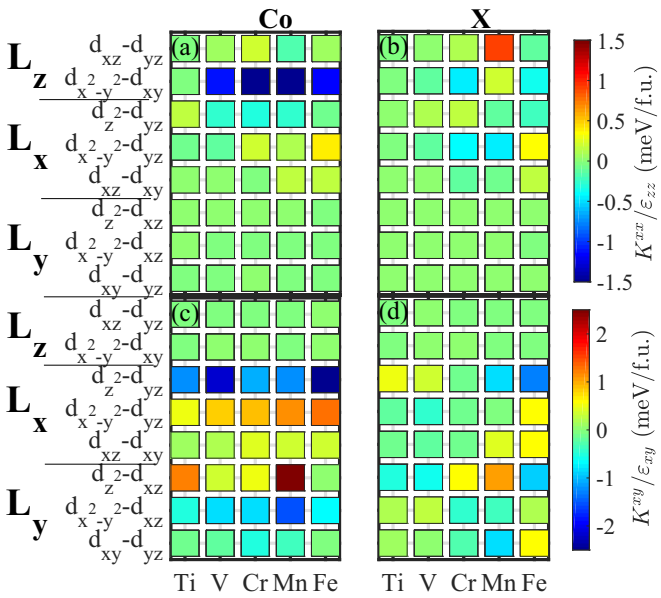

FIG. 4. (a) and (c) Co and (b) and (d) X-projected atomic-orbital-resolved contributions to strain-induced MCA, K^{xx}/ε_{zz} and K^{xy}/ε_{xy}, shown in the top and bottom panels, respectively. The left-hand ordinate shows the nonzero matrix elements of the three components of the orbital angular momentum operators, $\hat{L}_y$, $\hat{L}_x$, and $\hat{L}_z$.

the nonzero matrix elements of the three components of the orbital angular momentum operators, $\hat{L}_y$, $\hat{L}_x$, and $\hat{L}_z$.

For a cubic crystal structure subject to strain along z, the nonzero MCA constant, $K_{xx} = K_{yy}$, is given by

$$K^{xx} = -\vec{\tau}_{\mathrm{MCA}}^{[101]} \cdot \vec{e}_y = \langle \hat{\xi}(\hat{L}_x\hat{\sigma}_z - \hat{L}_z\hat{\sigma}_x)\rangle^{[101]}, \tag{23}$$

where the first and second terms correspond to the in-plane (xy-plane) and out-of-plane (z-axis) contributions of the strain-induced orbital moment accumulation, respectively. This is consistent with Figs. 4(a) and 4(b), where the magnetoelastic constant B_1 is dominated by the contribution of the strain-induced $\hat{L}_z$ orbital moment accumulation of the Co atoms. The $\langle d_{x^2-y^2}|\hat{L}_z|d_{xy}\rangle$ contribution to B_1 can be further decomposed into the spin-diagonal and spin-off-diagonal components, where, according to the second-order perturbation approach, the former (latter) yields positive (negative) contributions to the uniaxial MCA. Under a tensile strain along z we find a significant reduction of $\langle d_{x^2-y^2}|\hat{L}_z|d_{xy}\rangle$, resulting in a negative sign for B_1.

Similarly, using the spin-orbital torque expression and the strain-induced MCA under biaxial ε_{xy} strain, the magnetoelastic constant K^{xy} is given by the expression

$$K^{xy} = -\tfrac{1}{2}\vec{\tau}_{\mathrm{MCA}}^{[100]} \cdot \vec{e}_z = -\tfrac{1}{2}\langle \hat{\xi}(\hat{L}_x\hat{\sigma}_y - \hat{L}_y\hat{\sigma}_x)\rangle^{[100]}. \tag{24}$$

In the rotated frame of reference where the magnetization is along z, Eq. (24) shows that the spin-diagonal (spin-off-diagonal) matrix elements contribute to the orbital moment accumulation along y (x). Similar to the K^{xx} magnetoelastic constant, the main contribution to K^{xy} arises from the Co atoms, where the negative sign of B_2 is mainly due to the $\langle d_{z^2}|\hat{L}_x|d_{yz}\rangle$ orbital momentum matrix element. The sign reversal of K^{xy} for $X = \mathrm{Mn}$ is due to the relatively large positive contribution to the strain-induced orbital moment accumulation along the y axis.

V. CONCLUSION

In summary, we have presented a detailed first-principles study of the magnetoelastic and magnetostrictive properties of Co_2XAl full Heusler compounds that crystallize in the $L2_1$ structure. We described three computational approaches to calculate the magnetoelastic and magnetostriction tensor matrix elements. The first one is the well-known approach based on total energy calculations. The other two novel approaches are based on the torque [28] and spin-orbital torque [30] approaches, respectively. The latter two are computationally more efficient and allow the atomic and orbital decompositions of the magnetoelastic constants which can, in turn, elucidate the underlying atomic mechanisms. In addition, a general approach was presented to determine the average magnetostriction constants that is suitable for polycrystalline systems in terms of the magnetostriction tensor matrix elements. The results of the different computational approaches, using both the VASP and OPENMX packages, agree well, and they are also in good agreement with available experimental data.

ACKNOWLEDGMENTS

This work is supported by NSF ERC-Translational Applications of Nanoscale Multiferroic Systems (TANMS) Grant No. 1160504. We would like to thank N. Jones and K. B. Hathaway for useful discussions.

APPENDIX

The isotropic (volumetric) magnetostriction constants $\lambda_p^{(0)}$ and anisotropic magnetostriction constants $\lambda_{pq}^{(2)}$ can be expressed in terms of the magnetostriction tensor elements h_{ij}^{kl},

$$\lambda_1^{(0)} = \frac{1}{9}\sum_i \left(2h_{ii}^{zz} - h_{ii}^{xx} - h_{ii}^{yy}\right), \tag{A1a}$$

$$\lambda_2^{(0)} = \frac{1}{3\sqrt{3}}\sum_i \left(h_{ii}^{xx} - h_{ii}^{yy}\right), \tag{A1b}$$

$$\lambda_{11}^{(2)} = \frac{1}{9}\left(4h_{zz}^{zz} + h_{xx}^{xx} + h_{yy}^{yy} + h_{xx}^{yy} - 2h_{zz}^{xx} - 2h_{zz}^{yy} + h_{yy}^{xx} - 2h_{xx}^{zz} - 2h_{yy}^{zz}\right), \tag{A2a}$$

$$\lambda_{22}^{(2)} = \frac{1}{3}\left(h_{xx}^{xx} + h_{yy}^{yy} - h_{xx}^{yy} - h_{yy}^{xx}\right), \tag{A2b}$$

$$\lambda_{12}^{(2)} = \frac{1}{3\sqrt{3}}\left(2h_{zz}^{xx} - h_{xx}^{xx} - h_{yy}^{xx} - 2h_{zz}^{yy} + h_{xx}^{yy} + h_{yy}^{yy}\right), \tag{A2c}$$

$$\lambda_{21}^{(2)} = \frac{1}{3\sqrt{3}}\left(2h_{xx}^{zz} - h_{xx}^{xx} - h_{xx}^{yy} - 2h_{yy}^{zz} + h_{yy}^{xx} + h_{yy}^{yy}\right), \tag{A2d}$$

$$\lambda_{1p}^{(2)} = \frac{2}{3\sqrt{3}}\left(2h_{zz}^{p} - h_{xx}^{p} - h_{yy}^{p}\right), \quad p = yz, xz, xy, \tag{A2e}$$

$$\lambda_{2p}^{(2)} = \frac{2}{3}\left(h_{xx}^{p} - h_{yy}^{p}\right), \quad p = yz, xz, xy, \tag{A2f}$$

$$\lambda_{pq}^{(2)} = \frac{4}{3}h_p^q, \quad p, q = yz, xz, xy, \tag{A2g}$$

where we used the following expressions:

$$\int d\Omega d_{z^2}(x^2) = -\sqrt{\frac{4\pi}{45}}, \tag{A3a}$$

$$\int d\Omega d_{z^2}(y^2) = -\sqrt{\frac{4\pi}{45}}, \tag{A3b}$$

$$\int d\Omega d_{z^2}(z^2) = \sqrt{\frac{16\pi}{45}}, \tag{A3c}$$

$$\int d\Omega d_{x^2-y^2}(x^2) = \sqrt{\frac{4\pi}{15}}, \tag{A3d}$$

$$\int d\Omega d_{x^2-y^2}(y^2) = -\sqrt{\frac{4\pi}{15}}, \tag{A3e}$$

$$\int d\Omega d_{x^2-y^2}(z^2) = 0. \tag{A3f}$$

[1] A. Roy, R. Gupta, and A. Garg, Multiferroic magnetoelectric composites and their applications: multiferroic memories, Adv. Condens. Matter Phys. **2012**, 926290 (2012).

[2] É. du Trémolet de Lacheisserie, in *Magnetism: Materials and Applications*, edited by É. du Trémolet de Lacheisserie, D. Gignoux, and M. Schlenker (Springer, Boston, 2005), pp. 213–234.

[3] A. E. Clark, in *Ferromagnetic Materials*, edited by E. P. Wohlfarth (North-Holland, Amsterdam, 1980), Vol. 1, p. 531.

[4] A. V. Andreev, in *Handbook of Magnetic Materials*, edited by K. H. J. Bushow (Elsevier, Amsterdam, 1995), Vol. 8, p. 59.

[5] J. Atulasimha and A. B. Flatau, A review of magnetostrictive ironâgallium alloys, Smart Mater. Struct. **20**, 043001 (2011).

[6] R. Wu, L. Chen, and A. J. Freeman, First principles determination of magnetostriction in bulk transition metals and thin films, J. Magn. Magn. Mater. **170**, 103 (1997).

[7] D. Fritsch and C. Ederer, First-principles calculation of magnetoelastic coefficients and magnetostriction in the spinel ferrites $CoFe_2O_4$ and $NiFe_2O_4$, Phys. Rev. B **86**, 014406 (2012).

[8] I. Turek, J. Rusz, and M. Divis, Origin of the negative volume magnetostriction of the intermetallic compound $GdAl_2$, J. Alloys Compd. **431**, 37 (2007).

[9] R. Grössinger, R. Sato Turtelli, N. Mehmood, S. Heiss, H. Müller, C. Bormio-Nunes, Giant magnetostriction in rapidly quenched FeâGa? J. Magn. Magn. Mater. **320**, 2457 (2008).

[10] A. E. Clark, J.-H. Yoo, J. R. Cullen, M. Wun-Fogle, G. Petculescu, and A. Flatau, Stress dependent magnetostriction in highly magnetostrictive $Fe_{100-x}Ga_x$, $0< x <30$, J. Appl. Phys. **105**, 07A913 (2009).

[11] G. Petculescu, K. B. Hathaway, T. A. Lograsso, M. Wun-Fogle, and A. E. Clark, Magnetic field dependence of galfenol elastic properties, J. Appl. Phys. **97**, 10M315 (2005).

[12] A. E. Clark, J. B. Restorff, M. Wun-Fogle, D. Wu, and T. A. Lograsso, Temperature dependence of the magnetostriction and magnetoelastic coupling in $Fe_{100-x}Al_x$, $x = (14.1, 16.6, 21.5, 26.3)$ and $Fe_{50}Co_{50}$, J. Appl. Phys. **103**, 07B310 (2008).

[13] H. Zheng, J. Wang, S. E. Loand, Z. Ma, L. Mohaddes-Ardabili, T. Zhao, L. Salamanca-Riba, S. R. Shinde, S. B. Ogale, F. Bai, D. Viehland, Y. Jia, D. G. Schlom, M. Wuttig, A. Roytburd, and R. Ramesh, Multiferroic $BaTiO_3$-$CoFe_2O_4$ nanostructures, Science **303**, 661 (2004).

[14] T. Graf, C. Felser, and S. S. P. Parkin, Simple rules for the understanding of Heusler compounds, Prog. Solid State Chem. **39**, 1 (2011).

[15] C. Felser and A. Hirohata, *Heusler Alloys: Properties, Growth, Applications*, Springer Series of Materials Science Vol. 222 (Springer, Cham, 2016).

[16] S. Wurmehl, G. H. Fecher, H. C. Kandpal, V. Ksenofontov, and C. Felser, Investigation of Co_2FeSi: The Heusler compound with highest Curie temperature and magnetic moment, Appl. Phys. Lett. **88**, 032503 (2006).

[17] W. Wang, E. Liu, M. Kodzuka, H. Sukegawa, M. Wojcik, E. Jedryka, G. H. Wu, K. Inomata, S. Mitani, and K. Hono, Coherent tunneling and giant tunneling magnetoresistance in Co_2FeAl/MgO/CoFe magnetic tunneling junctions, Phys. Rev. B **81**, 140402(R) (2010).

[18] H. Liu, Y. Honda, T. Taira, K. Matsuda, M. Arita, T. Uemura, and M. Yamamoto, Giant tunneling magnetoresistance in epitaxial Co_2MnSi/MgO/Co_2MnSi magnetic tunnel junctions by half-metallicity of Co_2MnSi and coherent tunneling, Appl. Phys. Lett. **101**, 132418 (2012).

[19] K. Ullakko, Magnetically controlled shape memory alloys: A new class of actuator materials, J. Mater. Eng. Perform. **5**, 405 (1996).

[20] J. H. Wernick, G. W. Hull, J. E. Bernardini, and J. V. Waszczak, Superconductivity in ternary Heusler compounds, Mater. Lett. **2**, 90 (1983).

[21] Z. Wang, M. G. Vergniory, S. Kushwaha, M. Hirschberger, E. V. Chulkov, A. Ernst, N. P. Ong, R. J. Cava, and B. Andrei Bernevig, Time-Reversal-Breaking Weyl Fermions in Magnetic Heusler Alloys, Phys. Rev. Lett. **117**, 236401 (2016).

[22] I. Belopolski, K. Manna, D. S. Sanchez, G. Chang, B. Ernst, J. Yin, S. S. Zhang, T. Cochran, N. Shumiya, H. Zheng *et al.*, Discovery of topological Weyl fermion lines and drumhead surface states in a room temperature magnet, Science **365**, 1278 (2019).

[23] A. Sakai, Y. P. Mizuta, A. A. Nugroho, R. Sihombing, T. Koretsune, M.-T. Suzuki, N. Takemori, R. Ishii, D. Nishio-Hamane, R. Arita, and P. G. Satoru, Giant anomalous Nernst effect and quantum-critical scaling in a ferromagnetic semimetal, Nat. Phys. **14**, 1119 (2018).

[24] D. D. Koelling and B. N. Harmon, A technique for relativistic spin-polarised calculations, J. Phys. C: **10**, 3107 (1977).

[25] H. J. F. Jansen, Magnetic anisotropy, in *Science and Technology of Nanostructured Magnetic Materials*, edited by G. C. Hadjipanayis and G. A. Prinz (Plenum, New York, 1990), p. 349.

[26] M. Weinert, R. E. Watson, and J. W. Davenport, Total-energy differences and eigenvalue sums, Phys. Rev. B **32**, 2115 (1985).

[27] X. Wang, R. Wu, D. Wang, and A. J. Freeman, Torque method for the theoretical determination of magnetocrystalline anisotropy, Phys. Rev. B **54**, 61 (1996).

[28] F. Mahfouzi and N. Kioussis, First-principles study of the angular dependence of the spin-orbit torque in Pt/Co and Pd/Co bilayers, Phys. Rev. B **97**, 224426 (2018).

[29] F. Mahfouzi, J. Kim, and N. Kioussis, Intrinsic damping phenomena from quantum to classical magnets: An *ab initio* study of Gilbert damping in a Pt/Co bilayer, Phys. Rev. B **96**, 214421 (2017).

[30] F. Mahfouzi, R. Mishra, Po-Hao Chang, H. Yang, and N. Kioussis, Microscopic origin of spin-orbit torque in ferromagnetic heterostructures: A first-principles approach, Phys. Rev. B **101**, 060405(R) (2020)

[31] J. Joule, On a new class of magnetic forces, Ann. Elec. Magn. Chem. **8**, 219 (1842).

[32] C. Kittel, Physical theory of ferromagnetic domains, Rev. Mod. Phys. **21**, 541 (1949).

[33] E. W. Lee, Magnetostriction and magnetomechanical effects, Rep. Prog. Phys. **18**, 184 (1955).

[34] E. R. Callen and H. B. Callen, Static magnetoelastic coupling in cubic crystals, Phys. Rev. **129**, 578 (1963).

[35] G. Kresse and J. Furthmüller, Efficient iterative schemes for *ab initio* total-energy calculations using a plane-wave basis set, Phys. Rev. B **54**, 11169 (1996).

[36] G. Kresse and J. Furthmüller, Efficiency of *ab-initio* total energy calculations for metals and semiconductors using a plane-wave basis set, Comput. Mater. Sci. **6**, 15 (1996).

[37] T. Ozaki, Variationally optimized atomic orbitals for large-scale electronic structures, Phys. Rev. B **67**, 155108 (2003).

[38] T. Ozaki and H. Kino, Numerical atomic basis orbitals from H to Kr, Phys. Rev. B **69**, 195113 (2004).

[39] T. Ozaki and H. Kino, Efficient projector expansion for the *ab initio* LCAO method, Phys. Rev. B **72**, 045121 (2005).

[40] J. P. Perdew, K. Burke, and M. Ernzerhof, Generalized Gradient Approximation Made Simple, Phys. Rev. Lett. **77**, 3865 (1996).

[41] P. E. Blöchl, Projector augmented-wave method, Phys. Rev. B **50**, 17953 (1994).

[42] G. Kresse and D. Joubert, From ultrasoft pseudopotentials to the projector augmented-wave method, Phys. Rev. B **59**, 1758 (1999).

[43] N. Troullier and J. L. Martins, Efficient pseudopotentials for plane-wave calculations, Phys. Rev. B **43**, 1993 (1991).

[44] D. M. Ceperley and B. J. Alder, Ground State of the Electron Gas by a Stochastic Method, Phys. Rev. Lett. **45**, 566 (1980).

[45] J. P. Perdew and A. Zunger, Self-interaction correction to density-functional approximations for many-electron systems, Phys. Rev. B **23**, 5048 (1981).

[46] H. C. Kandpal, G. H. Fecher, and C. Felser, Calculated electronic and magnetic properties of the half-metallic, transition metal based Heusler compounds, J. Phys. D **40**, 1507 (2007).

[47] T. Graf, G. H. Fecher, J. Barth, J. Winterlik and C. Felser, Electronic structure and transport properties of the Heusler compound Co_2TiAl, J. Phys. D **42**, 084003 (2009).

[48] P. J. Webster and K. R. A. Ziebeck, Magnetic and chemical order in Heusler alloys containing cobalt and titanium, J. Phys. Chem. Solids **34**, 1647 (1973).

[49] T. Kanomata, Y. Chieda, K. Endo, H. Okada, M. Nagasako, K. Kobayashi, R. Kainuma, R. Y. Umetsu, H. Takahashi, Y. Furutani, H. Nishihara, K. Abe, Y. Miura, and M. Shirai, Magnetic properties of the half-metallic Heusler alloys Co_2VAl and Co_2VGa under pressure, Phys. Rev. B **82**, 144415 (2010).

[50] A. W. Carbonari, W. Pendl, Jr., R. N. Attili, and R. N. Saxena, Magnetic hyperfine fields in the Heusler alloys Co_2 YZ (Y = Sc, Ti, Hf, V, Nb; Z = Al, Ga, Si, Ge, Sn), Hyperfine Interact. **80**, 971 (1993).

[51] K. R. A. Ziebeck and P. J. Webster, A neutron diffraction and magnetization study of Heusler alloys containing Co and Zr, Hf, V or Nb, J. Phys. Chem. Solids **35**, 1 (1974).

[52] K. H. J. Buschow and P. G. van Engen, Magnetic and magneto-optical properties of heusler alloys based on aluminum and gallium, J. Magn. Magn. Mater. **25**, 90 (1981).

[53] M. H. P. Kameli and H. Salamati, Structural and magnetic properties of Co_2CrAl Heusler alloys prepared by mechanical alloying, J. Magn. Magn. Mater. **322**, 3443 (2010).

[54] Y. V. Kudryavtsev, V. N. Uvarov, V. A. Oksenenko, Y. P. Lee, J. B. Kim, Y. H. Hyun, K. W. Kim, J. Y. Rhee, and J. Dubowik, Effect of disorder on various physical properties of Co_2CrAl Heusler alloy films: Experiment and theory, Phys. Rev. B **77**, 195104 (2008).

[55] N. I. Kourova, A. V. Koroleva, V. V. Marchenkova, A. V. Lukoyanova, and K. A. Belozerova, Magnetic and electrical properties of the half metallic ferromagnets Co_2CrAl, Phys. Solid State **55**, 977 (2013).

[56] P. Nehla, Y. Kareri, G. D. Gupt, J. Hester, P. D. Babu, C. Ulrich, and R. S. Dhaka, Neutron diffraction and magnetic properties of $Co_2Cr_{1-x}Ti_xAl$ Heusler alloys, Phys. Rev. B **100**, 144444 (2019).

[57] A. Datta, M. Modak, and S. Banerjee, Magnetic properties of $Co_{2-x}Cr_{1+x}Al$ (x = 0, 0.4), in *3rd International Conference on Condensed Matter and Applied Physics (ICC-2019)*, edited by M. S. Shekhawat, S. Bhardwaj, and B. Suthar, AIP Conf. Proc. No. 2220 (AIP, New York, 2020), p. 110034.

[58] P. J. Webster, Magnetic and chemical order in Heusler alloys containing cobalt and manganese, J. Phys. Chem. Solids **32**, 1221 (1971).

[59] R. Y. Umetsu, K. Kobayashi, A. Fujita, R. Kainuma, and K. Ishida, Magnetic properties and stability of L21 and B2 phases in the Co_2MnAl Heusler alloy, J. Appl. Phys. **103**, 07D718 (2008).

[60] V. Jain, V. Jain, V. D. Sudheesh, N. Lakshmi, and K. Venugopalan, Electronic structure and magnetic properties of disordered Co_2FeAl Heusler alloy, in *Solid State Physics: Proceedings of the 58th DAE Solid State Physics Symposium 2013*, AIP Conf. Proc. No. 1591 (AIP, New York, 2014), p. 1544.

[61] S. Husain, S. Akansel, A. Kumar, P. Svedlindh, and S. Chaudhary, Growth of Co_2FeAl Heusler alloy thin films on Si(100) having very small Gilbert damping by ion beam sputtering, Sci. Rep. **6**, 28692 (2016).

[62] H. J. Elmers, S. Wurmehl, G. H. Fecher, G. Jakob, S. Felser, and G. Schonhense, Field dependence of orbital magnetic moments in the Heusler compounds Co_2FeAl and $Co_2Cr_{0.6}Fe_{0.4}Al$, Appl. Phys. A **79**, 557 (2004).

[63] R. M. Bozorth, *Ferromagnetism* (Van Nostrand, New York, 1951), p. 441.

[64] J. Kubler, G. H. Fecher, and C. Felser, Understanding the trend in the Curie temperatures of Co_2-based Heusler compounds: *Ab initio* calculations, Phys. Rev. B **76**, 024414 (2007).

[65] S.-C. Wu, G. H. Fecher, S. S. Naghavi, and C. Felser, Elastic properties and stability of Heusler compounds: Cubic Co_2YZ compounds with L21 structure, J. Appl. Phys. **125**, 082523 (2019).

[66] J. J. Qiu, G. C. Han, W. K. Yeo, P. Luo, Z. B. Guo, and T. Osipowicz, Structural and magnetoresistive properties of magnetic tunnel junctions with half-metallic Co_2MnAl, J. Appl. Phys. **103**, 07A903 (2008).

[67] M. Gueye, B. M. Wague, F. Zighem, M. Belmeguenai, M. S. Gabor, T. Petrisor, Jr., C. Tiusan, S. Mercone, and D. Faurie, Bending strain-tunable magnetic anisotropy in Co_2FeAl Heusler thin film on Kapton, Appl. Phys. Lett. **105**, 062409 (2014).